



## Thinking of bosentan repurposing – A study on dehydration and amorphization

Anna Krupa<sup>a,\*</sup>, Florence Danède<sup>b</sup>, Agnieszka Węgrzyn<sup>c</sup>, Dorota Majda<sup>c</sup>, Jean-François Willart<sup>b</sup>

<sup>a</sup> Jagiellonian University, Medical College, Faculty of Pharmacy, Department of Pharmaceutical Technology and Biopharmaceutics, 9 Medyczna Street, 30-688 Cracow, Poland

<sup>b</sup> University of Lille, CNRS, INRAE, Centrale Lille, UMR 8207, UMET – Unité Matériaux et Transformations, F-59000 Lille, France

<sup>c</sup> Jagiellonian University, Faculty of Chemistry, 2 Gronostajowa Street, 30-387 Cracow, Poland

### ARTICLE INFO

#### Keywords:

Bosentan  
Vitrification  
Amorphization kinetics  
Ball milling  
Dehydration  
Dissolution

### ABSTRACT

New clinical indications for an orphan drug bosentan are prompting the improvement of the drug formulation. Since bosentan is available as monohydrate, the information on its anhydrous form together with the assessment of its glass forming ability is necessary when developing enabling formulations. The aim of this research was, therefore, to analyze the phenomena occurring upon dehydration and amorphization of bosentan. The anhydrous form was obtained by a thermal treatment of the monohydrate and characterized for the first time using DSC and XRD. Two stable amorphous forms were prepared by cooling of the melt and high energy ball milling ( $T_g = 82$  °C). The chemical stability of milled bosentan was evaluated using ATR-IR and <sup>1</sup>H NMR as well. The kinetics of bosentan amorphization was established. It was stated that bosentan could be easily amorphized. Importantly, even if the system was semiamorphous, there was no recrystallization while heating. The concentration–time curves recorded in biorelevant media, confirmed the beneficial effect of amorphization on the dissolution of bosentan. Yet, the amorphous form recrystallized into the monohydrate form in the gastric milieu. This phenomenon was accompanied by a reversible color change from yellow, which is typical of bosentan glass, to creamywhite that is characteristic of the crude crystalline drug

### 1. Introduction

Bosentan is a dual endothelin receptor (ET<sub>A</sub>, ET<sub>B</sub>) antagonist of non-peptide, pyrimidine ring based structure and a chemical name: 4-*tert*-butyl-N-[6-(2-hydroxy-ethoxy)-5-(2-methoxy phenoxy)[2, 2']-bipyrimidin-4-yl]-benzene sulphonamide. In 2001, it was approved as an orphan drug for the oral therapy of hereditary and idiopathic pulmonary arterial hypertension (PAH) and chronic thromboembolic pulmonary hypertension (Enevoldsen et al., 2020). Two years later, the designation for the oral treatment of systemic sclerosis was introduced in the orphan designation of this drug. In 2014, bosentan was withdrawn from the European list of the orphan drugs, but it still keeps this designation in PAH in the US, Japan and Australia. Nowadays, brand or generic prescription products in the form of tablets loaded with 62.5 mg or 125 mg of bosentan are available. They are usually administered twice a day. Twenty years of clinical experience provided the evidence that apart from side effects typical of vasodilators, bosentan is safe and the chronic oral therapy is, in general, well-accepted by patients.

Since the dysfunction of endothelin may be involved in the pathogenesis of various diseases, several case reports have been published, and multiple clinical studies have been established with the aim to identify new indications for bosentan (Enevoldsen et al., 2020). Among them there are idiopathic pulmonary fibrosis (King et al., 2011), metastatic melanoma (Kefford et al., 2010), skin ulcers in diabetic microangiopathy (Álvarez Reyes et al., 2011), pulmonary sarcoidosis (clinicaltrialsregister.eu) or multiple sclerosis (Hostenbach et al., 2019). Recently, the suitability of bosentan for the pharmacotherapy of severe acute respiratory syndrome coronavirus 2 (SARS-CoV-2) has also been suggested (Javor and Salsano, 2020; Sanghavi et al., 2021).

This shows a high interest in the repurposing of this drug. From biopharmaceutical point of view, bosentan is poorly soluble in water (less than 2 µg/mL) BCS class II drug, which means that its bioavailability after oral administration is solubility-limited. Indeed, the bioavailability of bosentan is low, i.e. 49.8 % (Enevoldsen et al., 2020). These features prompt to develop enabling formulations that could enhance its *in vivo* performance (Schittny et al., 2020). A common

\* Corresponding author.

E-mail address: [a.krupa@uj.edu.pl](mailto:a.krupa@uj.edu.pl) (A. Krupa).

<https://doi.org/10.1016/j.ijpharm.2022.121846>

Received 28 January 2022; Received in revised form 14 May 2022; Accepted 18 May 2022

Available online 21 May 2022

0378-5173/© 2022 The Author(s). Published by Elsevier B.V. This is an open access article under the CC BY license (<http://creativecommons.org/licenses/by/4.0/>).

approach is by transforming the crystalline poorly soluble drug into the amorphous counterpart of better solubility. Supersaturated solutions of the amorphous drug formed in the gastrointestinal fluids, creating a high concentration gradient between the lumen and the blood stream, could accelerate its absorption. In consequence, the bioavailability of the drug may increase and the drug dose may be reduced (Fong et al., 2017; Krupa et al., 2016; Krupa et al., 2017a).

To achieve this goal, Panda et al., 2016 proposed the preparation of ternary solid dispersions by fusing bosentan with a mixture of lipid based surfactants (Gelucire 50/13) and a nonionic polyoxyethylene–polyoxypropylene copolymer (Poloxamer 188). This melt was adsorbed on porous amorphous particles of silicon dioxide (Sylysia 350), and finally compacted to form tablets of immediate release. Recently, Kendre et al., 2021 proposed the fabrication of binary solid dispersions by combining bosentan with an amphiphilic co-polymer (Soluplus) in a solvent evaporation method. These formulations were used to prepare buccoadhesive tablets of enhanced drug solubility. Although the development of solid dispersion to enhance the performance of bosentan have already been undertaken, there is still a lack of understanding of the fundamental phenomena, occurring upon vitrification of bosentan. Moreover, the dehydration of bosentan monohydrate has not been studied so far. As a result, there is lack of information either on the impact that dehydration conditions may have on the properties of the anhydrous form or on the stability of the amorphous form. Thus, a thorough knowledge of these aspects is crucial to optimize the manufacturing of enabling formulations loaded with bosentan and to predict their stability upon storage. Such an approach could accelerate the design of new dosage forms necessary to meet the needs of patients treated with bosentan in new clinical indications.

The aim of this study was to assess the opportunity to dehydrate bosentan monohydrate in order to obtain the anhydrous form and to assess the glass forming ability of this drug. In particular, this research was focused on: (i) the development of anhydrous form of bosentan from monohydrate by thermal treatment, (ii) the assessment of the impact that dehydration conditions may have on the properties of the anhydrous form, (iii) its vitrification by quenched cooling, (iv) its amorphization in the solid state by high energy ball milling at ambient conditions, (v) the assessment of the impact that the amorphization of bosentan may have on its dissolution in biorelevant media.

The behavior of bosentan monohydrate subjected to dehydration by heating was examined using differential scanning calorimetry (DSC) and thermogravimetric analysis (TGA) in conjunction with hot stage X-ray powder diffraction (XRD) to establish if new polymorphs were formed under such a processing. ATR-IR together with  $^1\text{H}$  NMR spectroscopy were applied with the aim to identify chemical changes in the structure of bosentan that may be induced by either thermal treatment or mechanical activation of the drug. The impact of milling on both structural state and dissolution was also analyzed. Since the recrystallization of the amorphous form of the drug upon dissolution may occur, factors that could be responsible for this phenomenon were investigated. If the recrystallization of the amorphous form was stated, the properties of the precipitate were assessed using scanning electron microscopy (SEM), XRD and DSC studies.

## 2. Materials and methods

Bosentan monohydrate ( $M_w = 569.63$  g/mol,  $\log P = 3.7$ ) was kindly donated by Polpharma S.A. (Starogard Gdański, Poland). Potassium dihydrogen phosphate, disodium hydrogen phosphate and sodium chloride were purchased from Avantor Performance Materials Poland (Gliwice, Poland). All of these reagents were of analytical grade. The 50 % acetic acid for HPLC was supplied by Sigma-Aldrich Co. (St. Luis, MO, USA). Acetonitrile for HPLC of isocratic grade was purchased from Witko (Łódź, Poland). Water was obtained from a Milli-Q Elix Essential water purification system of Millipore Corporation (Merck, Warsaw, Poland).

### 2.1. Milling protocol

High energy ball milling was carried out at room temperature (RT) using a planetary ball mill Pulverisette 7, Fritsch (Idar-Oberstein, Germany). The samples (1.1 g of bosentan monohydrate) were placed in milling jars of 45 mL with seven milling balls of 1 cm in diameter. Both the milling jars and the milling balls were made of zirconium oxide leading to a ball to sample weight ratio of 75:1. The rotational speed of the solar disc was set at 400 rpm. The milling was performed for 2 min, 5 min, 10 min, 15 min, 20 min, 30 min, 40 min, 60 min, 120 min, 180 min, 240 min and 360 min. For milling periods longer than 20 min, the milling time of 20 min was alternated with 10 min-pause periods to avoid overheating of the samples.

### 2.2. Vitrification of bosentan by cooling of the melt

A sample of bosentan monohydrate (3–5 mg) was placed in a DSC pan. Three pan configurations were used: open standard or  $T_{\text{zero}}$  made of aluminum and hermetically sealed stainless steel O-ring pan. The following heating–cooling–heating protocol was applied with the use of a differential scanning calorimeter DSC Q1000 (TA Instruments, Guyancourt, France):

heating: 20 °C → 130 °C (5 °C/min),

cooling: 130 °C → 20 °C (50 °C/min).

Other operating parameters used upon cooling of the melt were described in a DSC section (2.5.).

### 2.3. Particle morphology

The samples of powder were adhered to a holder by double-sided copper tape. Their surface was coated with carbon using a 208 HR carbon sputter coater (Cressington Scientific Instruments, Watford, UK). Then, their morphology was analyzed by a scanning electron microscope (SEM) Hitachi S-4700 (Japan). The images were taken at the magnification of 250 × and 2000 ×.

### 2.4. X-ray powder diffraction (XRD)

The experiments were carried out with a PanAnalytical X'Pert PRO MPD diffractometer (Almelo, the Netherlands), equipped with X'Celerator detector. For the measurements carried out at RT, the samples were placed into Lindemann glass capillaries of 0.7 mm in diameter (Hilgenberg GmbH, Masfeld, Germany). The capillaries were installed on a rotating sample holder to avoid any artifacts due to preferential orientations of crystallites. The high temperature measurements were performed in Bragg-Brentano  $\theta$ - $\theta$  geometry. The samples were placed in an Anton Paar TTK 450 chamber under vacuum. All samples were exposed to X-ray radiation ( $\lambda_{\text{Cu}} - \text{K}\alpha$ ) with the wavelength of 1.540 Å. The diffractograms were recorded from 5 to 40° or 60°, with a counting time of 50 sec/point and a measuring step of 0.0167°.

### 2.5. Differential scanning calorimetry (DSC)

A differential scanning calorimeter DSC Q1000 (TA Instruments, Guyancourt, France) equipped with a refrigerated cooling system was used to characterize solid-state properties of bosentan. The temperature and enthalpy readings were calibrated, using pure indium at the same scan rates as those used in all the experiments. Samples (3–5 mg) were placed in either hermetic O-ring sealed stainless steel pans or open aluminum pans (container with no lid) to facilitate the evaporation of water. During the measurement, the calorimeter head was purged with highly pure nitrogen gas (50 mL min<sup>-1</sup>). The scans were performed with a heating rate of 5 °C/min which appeared to be a good compromise between resolution and intensity of enthalpic events. Samples in open pans were scanned from 20 °C to 130 °C while those in hermetic pans were scanned from 20 °C to 250 °C.

## 2.6. Thermogravimetric analysis (TGA)

The thermogravimetric analyses were carried out using a Q500 TGA (TA Instruments, Guyancourt, France). Samples were placed in open aluminum pans and the furnace was flushed with a highly pure nitrogen gas (50 mL/min). The temperature reading was calibrated using Curie points of alumel and nickel, while the mass reading was calibrated using balance tare weights provided by the manufacturer. All TGA scans were performed at 5 °C/min.

## 2.7. ATR-IR studies

Attenuated Total Reflectance-Infrared spectroscopy (ATR-IR) measurements were carried on Nicolet iS5 spectrometer (Thermo Scientific) equipped with iD3 ATR with ZnSe crystal window, in the range of 4000–525  $\text{cm}^{-1}$  with a resolution of 2  $\text{cm}^{-1}$  and a total of 64 scans.

## 2.8. $^1\text{H}$ NMR studies

$^1\text{H}$  nuclear magnetic resonance (NMR) spectra were recorded at 21 °C using a FT-NMR 500 MHz (JNM-ECZR500 RS1 v. ECZR, JEOL, Japan) spectrometer. Ten milligrams of the sample were dissolved in 0.75 mL of dimethylsulfoxide ( $\text{DMSO}-d_6$ ). The solutions were placed in 5-mm diameter NMR tubes and spectra were recorded. The peaks typical of  $\text{DMSO}-d_6$  and water were visible at 2.50 ppm and at 3.35 ppm respectively.

## 2.9. Saturation solubility studies

An access amount of bosentan monohydrate was placed into Eppendorf test tubes and 1 mL of phosphate buffer (PBS) of pH = 6.8, fasted or fed simulated intestinal fluid (FaSSIF, FeSSIF Biorelevant.com Ltd., London, UK) of pH = 6.5 or of pH = 5.0 was added. The samples were shaken using a laboratory thermomixer (uniTHERMIX 2 pro, LLG Labware, Meckenheim, Germany) at 37 °C and 500 rpm for 48 h. Then, they were centrifuged (uniCFUGES, LLG Labware, Meckenheim, Germany), filtered ( $\varnothing = 0.45 \mu\text{m}$ ) and diluted. The concentration of bosentan dissolved was determined using an HPLC-DAD method described below. Each analysis was performed in triplicate. Mean values and corresponding standard deviations were calculated.

## 2.10. Dissolution studies

The dissolution of crude and milled bosentan was studied in non-sink conditions using three different media, i.e. simulated gastric fluid (SGF, Ph. Eur. 10th Ed., pH = 1.20) without pepsin, phosphate buffer of pH = 6.80 (PBS), fasted or fed state simulated intestinal fluid of pH = 6.50 or pH = 5.00 respectively (FaSSIF, or FeSSIF, Biorelevant.com Ltd., London, UK). The tests were performed at 37 °C  $\pm$  0.5 °C. An automated pharmacopoeial paddle dissolution apparatus - Hanson Research Dissolution Station Vision Elite 8 with an autosampler Visione Auto-Plus™ Maximizer and a sample collector AutoFill™ device (Chatsworth, CA, USA) equipped in a set of small vessels (150 mL) was used. Each test was performed using 20 mg of bosentan and 100 mL of SGF, PBS or biorelevant fluids. The paddle rotation speed was set at 75 rpm. The samples of 2 mL were withdrawn for 120 min and the same amount of the replace medium was added. The samples were transferred into the test tubes containing acetonitrile (0.2 mL – 2 mL). Then, they were vortexed (Reax Control, Heidolph, Schwabach, Germany) and filtered ( $\varnothing = 0.45 \mu\text{m}$ ) directly into HPLC vials. The concentration of bosentan dissolved was determined using HPLC method described below. Mean values ( $n = 3$ ) in  $\mu\text{g mL}^{-1}$  and corresponding standard deviations were calculated.

## 2.11. HPLC-DAD method

The concentration of bosentan dissolved was determined using a HPLC system Agilent 1260 Infinity (Waldbronn, Germany) connected to a diode array detector (DAD). The samples were filtered through a nylon syringe filter ( $\varnothing = 0.45 \mu\text{m}$ ). They were analyzed using a reversed phase LC column InfinityLab Poroshell 120EC-C18 (4.6  $\times$  100 mm; particle size 4  $\mu\text{m}$ ) with a guard column InfinityLab Poroshell 120-EC-C18 (4.6  $\times$  5 mm, particle size 4  $\mu\text{m}$ ). The injection volume was 5  $\mu\text{L}$ . The mobile phase was composed of acetonitrile and 0.1 % (v/v) acetic acid mixed in 60:40 (v/v) ratio (isocratic elution). The flow rate was 0.8  $\text{mL min}^{-1}$ . The column oven temperature was set at 25 °C. The signal of bosentan was detected at the wavelength of 267 nm.

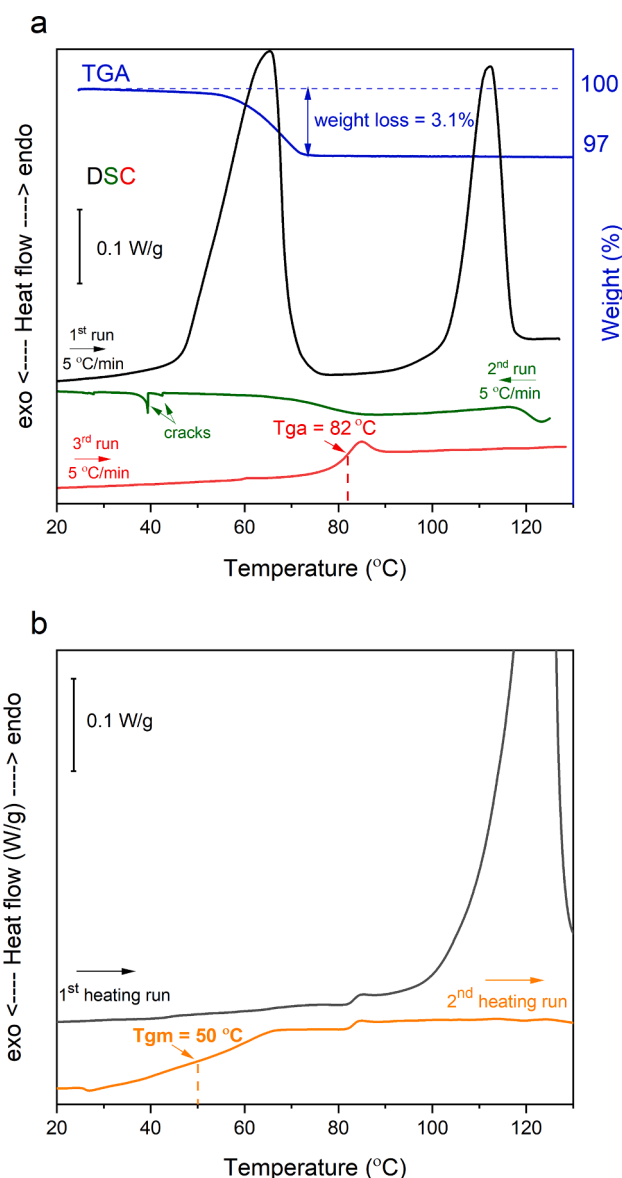


Fig. 1. DSC thermograms of crude bosentan monohydrate (BOS) recorded upon heating-cooling-reheating cycle in: (a) open aluminum pans; (b) close hermetic stainless steel pans with O-ring seal. Thermogravimetric curve of crude BOS monohydrate was also shown in (a).

### 3. Results and discussion

#### 3.1. Bosentan anhydrous obtained by dehydration of monohydrate

Fig. 1a shows the TGA scan (5 °C/min) of bosentan monohydrate recorded in an open pan. It shows a mass loss of 3.1 % between 55 and 75 °C, which corresponds exactly to the mass ratio between bosentan ( $M_w \sim 570$  g/mol) and water ( $M_w \sim 18$  g/mol) in the monohydrate. This mass loss could, thus, be attributed to the total dehydration of the monohydrate.

The heating DSC scan recorded in the same conditions (open pan, 5 °C/min) is also reported in Fig. 1a (run 1). It shows two endotherms. The first one is broad and occurs exactly at the temperature range [55 °C; 75 °C] where the water loss has been detected by TGA. It, thus, corresponds to the dehydration of the monohydrate. The second endotherm at  $T_m = 112$  °C, reflects the melting of the anhydrous material whose melting enthalpy is  $\Delta H_m = 49$  J/g. This melting indicates that an anhydrous crystalline form has been produced during the previous dehydration stage.

Fig. 2 shows the X-ray diffraction patterns of bosentan monohydrate recorded at different temperatures. The sample was placed in an open aluminum plate under vacuum to allow water release. At room temperature (RT), the X-ray diffraction pattern shows many Bragg peaks, indicating the crystalline character of the material. The position of these Bragg peaks is perfectly coherent with the  $P2_1/c$  structure reported for bosentan monohydrate (Kaur et al., 2013). At 75 °C (i.e.: just above the dehydration range), the diffractogram is strongly modified. Some Bragg peaks disappear while many others develop. This indicates that the water loss has induced the formation of a crystalline anhydrous form. After heating to 130 °C (i.e.: above the second endotherm seen in the run 1 of Fig. 1a), all Bragg peaks disappeared, which confirms the melting of the sample.

Fig. 3 shows the diffractograms of the anhydrous form obtained at 75 °C, after cooling it back to RT in vacuum conditions, and then just after breaking vacuum. Clearly, at RT and under vacuum, the x-ray diffraction pattern remains characteristic of the anhydrous form while after breaking vacuum the diffractogram typical of the monohydrate is rapidly restored (in less than 15 min). As a result, the anhydrous form is highly hygroscopic, and therefore, it can only be observed at RT in dry conditions.

Physical transformations induced by the dehydration of hydrates have been widely studied (Petit and Coquerel, 1996; Galwey, 2000). It appears that these transformations can produce either anhydrous

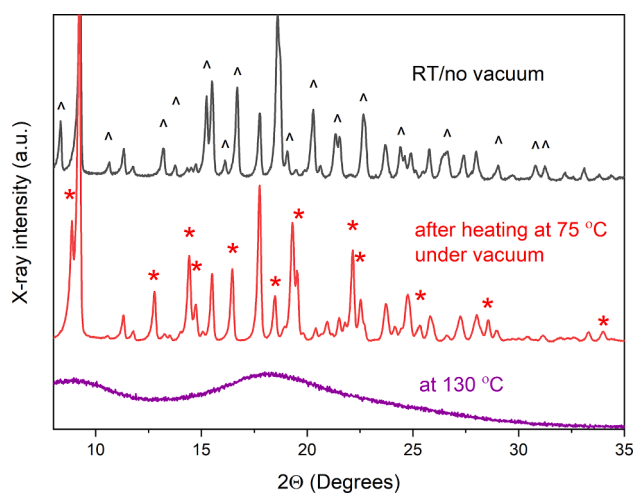


Fig. 2. Diffractograms of crude bosentan monohydrate recorded at (from top to bottom): room temperature (RT); after heating up to 75 °C under vacuum, and after heating up to 130 °C. The heating was performed in a diffractometer. Peaks which intensity changed upon heating were marked.

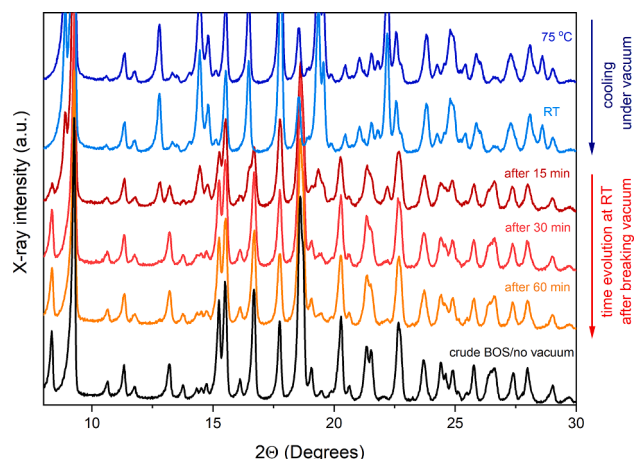


Fig. 3. Diffractograms of bosentan monohydrate recorded (from top to bottom): after drying at 75 °C under vacuum, after cooling back to RT under vacuum, and at different periods of time (15, 30 et 60 min) after breaking vacuum. The diffractogram of crude bosentan monohydrate (BOS) at ambient conditions is reported for comparison.

crystalline forms or an amorphous counterpart (Saleki-Gerhardt et al., 1995; Garnier et al., 2002; Willart et al., 2002). Moreover, it has been shown that the nature of the transformation often depends on the dehydration conditions (Garnier et al., 2008), and in particular, on the dehydration rate (Willart et al., 2003). In the present study, bosentan monohydrate was dehydrated in a variety of thermal treatments using fast and slow heating rates. In all these cases, the dehydration was found to produce the same anhydrous crystalline form, indicating that the nature of the transformation does not seem to depend on the dehydration rate.

#### 3.2. Vitrification of bosentan by quench cooling

Fig. 1a shows the cooling (5 °C/min) DSC scan (run 2nd) of the liquid bosentan obtained at the end of the 1st run. It shows no exothermic crystallization event, which provides the evidence that bosentan can be easily undercooled. We can also note the occurrence of tiny exothermic spikes around 40 °C, which are characteristic of the sudden formation of cracks in the glassy material. These cracks were observed for instance in griseofulvin (Willart et al., 2017), ibuprofen (Dudognon et al., 2008) and indomethacin (Bhugra et al., 2008). They were attributed to very strong mechanical stresses, which developed in these amorphous solids far below  $T_g$ . While they do not correspond to a structural change of the sample, they can have a strong repercussion on the recrystallization propensity of the material upon reheating (Willart et al., 2017). The 3rd run corresponds to the heating (5 °C/min) DSC scan of the quenched liquid. It shows a clear  $C_p$  jump ( $\Delta C_p = 0.47$  J/°C/g) typical of a glass transition at  $T_g = 82$  °C. Above  $T_g$ , no exothermic recrystallization could be detected, showing that bosentan is a very good glass former with a high stability against recrystallization.

Interestingly, we can note that the glass transition of bosentan ( $T_g = 82$  °C) is unusually close to the melting point ( $T_m = 112$  °C) of the anhydrous crystalline form. Considering the empirical law (Gutzow et al., 2011) which states that  $T_g$  is generally not far from  $2/3 T_m$ :

$$T_g = 2/3 T_m \quad (T_m \text{ in Kelvin}) \quad \text{Eq. (1)}$$

the melting point of anhydrous bosentan would rather be expected around 260 °C. Such a situation is reminiscent of that detected in trehalose whose form  $\alpha$  obtained by slow dehydration of the dihydrate form was found to melt only 5 °C above  $T_g$ . However, in that case, the recrystallization of the melt upon further heating produced a more stable crystalline form (called  $\beta$ ), which then melted around 220 °C, so in agreement with the empirical law (1). By analogy with trehalose, the existence of an anhydrous crystalline form of bosentan more stable than



that produced by the dehydration of the monohydrate can, thus, be suspected. However, up to know, there was no recrystallization of the melted anhydrous form observed upon heating (5 °C/min) up to 290 °C where the chemical degradation of bosentan started (Krupa et al., 2017b).

Fig. 1b shows heating (5 °C/min) DSC scans of bosentan monohydrate encapsulated in a close hermetic pan with O-ring seal. The 1st run corresponds to the crystalline monohydrate. Due to hermetic conditions, no dehydration endotherm is observed around 60 °C. We only observe a single endotherm at  $T_m = 110$  °C, illustrating the melting of the monohydrate. The 2nd run corresponds to the quenched liquid obtained by cooling (5 °C/min) the melt produced at the end of the 1st run. It shows no sign of melting, which indicates that the melt was successfully quenched. We can only observe a large Cp jump, revealing the glass transition at  $T_g = 50$  °C, i.e. 32 °C below that of the anhydrous glass (Fig. 1a – run 3rd). Such a depression of the glass transition was due to the plasticization of amorphous bosentan by water molecules previously involved in the crystalline monohydrate. The Gordon-Taylor theory (Gordon et al., 1977) applied to the bosentan/water binary mixture indicates that the glass transition temperature corresponding to the monohydrate composition is located between 68 °C and 34 °C. These two values have been obtained by considering respectively the glass transition characteristics of HDA and LDA ices [respectively Low Density and High Density Amorphous ices] (Amann-Winkel et al., 2013). These predictions are thus, perfectly coherent with the observed glass transition of the amorphous bosentan monohydrate which appears to occur in this very temperature range.

### 3.3. Solid state amorphization of bosentan by ball milling

The structural and thermodynamic evolution of bosentan monohydrate upon milling have been investigated by XRD and DSC. Fig. 4a shows the X-ray diffraction patterns of bosentan monohydrate recorded after different milling times ranging from 0 to 360 min. In this experiment, freshly milled samples were placed in Lindemann glass capillaries ( $\varnothing = 0.7$  mm) and diffractograms were collected at RT. These results indicate that the Bragg peaks characteristic of the monohydrate decrease progressively with the increasing milling time. This strongly suggests that bosentan monohydrate undergoes amorphization upon milling. We also noted a broadening of Bragg peaks, which could be attributed to the size reduction of the remaining crystallites, fragmented by the mechanical chocks. After 120 min of milling, all Bragg peaks have totally disappeared and the X-ray diffraction pattern looked like that of an amorphous material. Moreover, any further evolution of the diffractograms could be observed for longer milling.

The heating (5 °C/min) DSC scans of the previously milled samples are reported in Fig. 4b. They were recorded using open DSC pans, after 15 min of annealing at 60 °C to evaporate water. For milling times up to 120 min, we observe a progressive development of a Cp jump at 82 °C. This Cp jump is characteristic of the glass transition of dry amorphous bosentan and it proves a gradual amorphization of the monohydrate upon milling that has already been suggested by XRD (Fig. 4a). We can also note, the concomitant decrease in the melting endotherm of the anhydrous crystalline form of bosentan, arising from the dehydration of the fraction of bosentan monohydrate, which has not been yet amorphized by milling. After 120 min of milling, the Cp jump at  $T_g$  was identical to that of the glassy bosentan obtained by the quenching of the melt (Fig. 1a – 3rd run), and the melting endotherm of bosentan anhydrous disappeared. These facts indicate that bosentan underwent a solid state transformation from crystal to glass upon milling. No more evolution of the thermogram could be observed for longer milling.

It must be noted that fully amorphous bosentan obtained after 120 min of milling did not recrystallize upon milling. Such a stability against recrystallization is really unusual for a milling induced amorphous material and it has only been observed in a very rare cases, e.g.: lactulose (Ngonu et al., 2019) and trehalose after a very long milling process of 100 h (Willart et al., 2007). Interestingly, so high stability was also effective in the course of the amorphization process itself since no sign of recrystallization could be observed for shorter milling times when the amorphization was only partial. The absence of recrystallization in the course of the amorphization process is quite exceptional and, to our knowledge, was never observed in any other material. This is probably due to the fact that the crystalline structure of the initial monohydrate and that of the anhydrous form towards which the recrystallization is expected to occur are very different. In these conditions, remaining monohydrate crystallites cannot act as seeds to promote the recrystallization of the anhydrous form upon heating. Moreover, the local order in the amorphous bosentan obtained by milling may be reminiscent of the monohydrate structure, and thus, not favorable to induce the recrystallization of the anhydrous form.

The amorphization kinetics of bosentan upon milling is reported in Fig. 5. Amorphous fractions ( $X_{am}$ ) were calculated on the basis of DSC data, according to Eq. (2), where  $\Delta H_m$  is the enthalpy of melting of non-milled anhydrous bosentan and  $\Delta H_m^{milled}$  is the enthalpy of melting of crystalline bosentan in ball milled samples.

$$y = 1 - (\Delta H_m^{milled} / \Delta H_m) \text{ Eq. (2)}$$

The amorphization kinetics upon milling generally obeys an exponential relaxation law given by Eq. (3):

$$X_{am}(t) = 1 - \exp(-t/\tau) \text{ Eq. (3)}$$

Where  $\tau$  is the relaxation time of the amorphization process. The

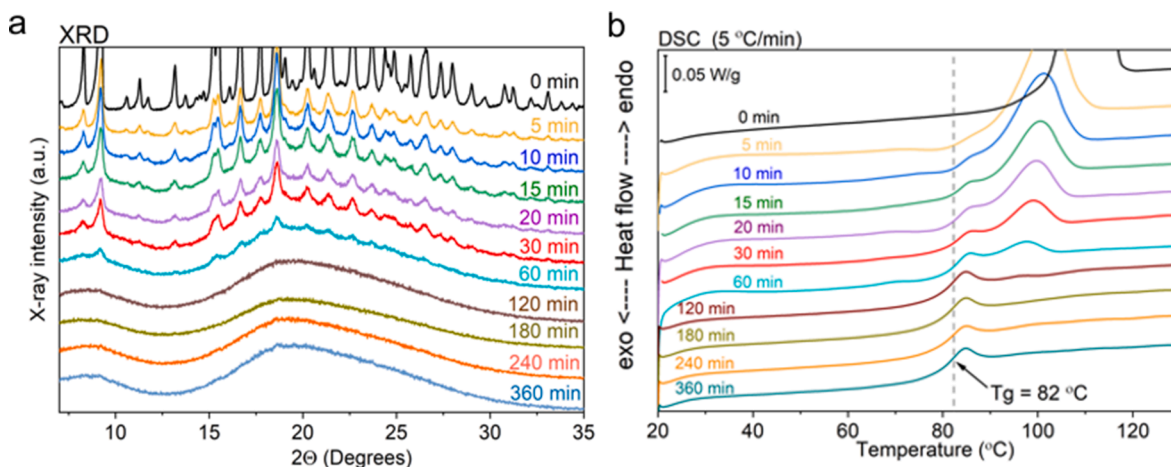
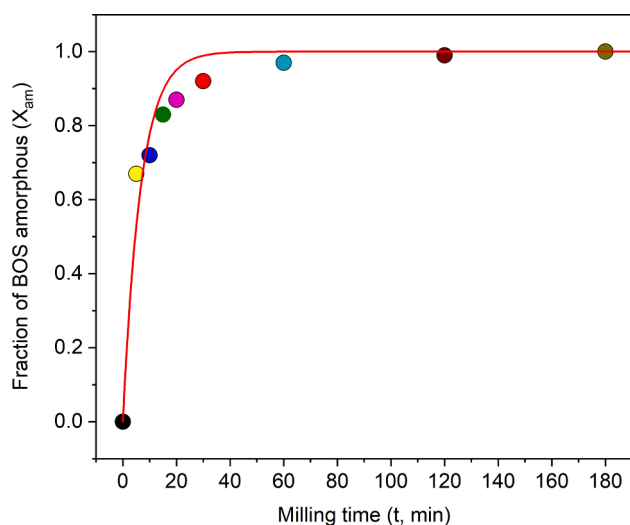


Fig. 4. X-ray powder diffraction patterns (a) and heating (5 °C/min) DSC scans (b) of bosentan monohydrate recorded after different milling times. XRD patterns were recorded just after milling. DSC scans were recorded after a 15 min annealing at 60 °C to remove water from the sample.



**Fig. 5.** Amorphization kinetics of bosentan monohydrate upon high energy ball milling. Fitting of the experimental curve to the exponential relaxation law (solid red line). (For interpretation of the references to color in this figure legend, the reader is referred to the web version of this article.)

solid line in Fig. 5 corresponds to the best fit of Eq. (3) to the data. It describes pretty well the data and indicates that the relaxation time of the amorphization process is close to 6.6 min. Noteworthy, this time is very short compared to that measured for other compounds milled exactly in the same conditions [chlorhexidine dihydrochloride (Elisei et al., 2018)], which confirms the great ease of bosentan to amorphize upon milling.

Since mechanical activation of a compound may induce degradation of the sample or initiate numerous chemical reactions,  $^1\text{H}$  NMR studies in  $\text{DMSO-}d_6$  (Fig. S1) together with solid state ATR-IR spectra (Fig. S2) were recorded in order to identify chemical changes in bosentan. The  $^1\text{H}$  NMR spectrum of bosentan amorphized by milling for 240 min was the same as that of the reference crystalline sample (Fig. S1). Moreover, even after a year of storage at ambient conditions, the spectrum of the amorphous sample was still identical as that of the crude drug. The same was true for ATR-IR spectrum of fully amorphous milled bosentan (Fig. S2). Apart from a characteristic broadening of bands, typical of the amorphous materials, both spectra showed the same features. Thus, the mechanical activation of bosentan upon high energy ball milling has no detrimental effect on the chemical stability of bosentan.

### 3.4. Impact of amorphization on dissolution of bosentan monohydrate

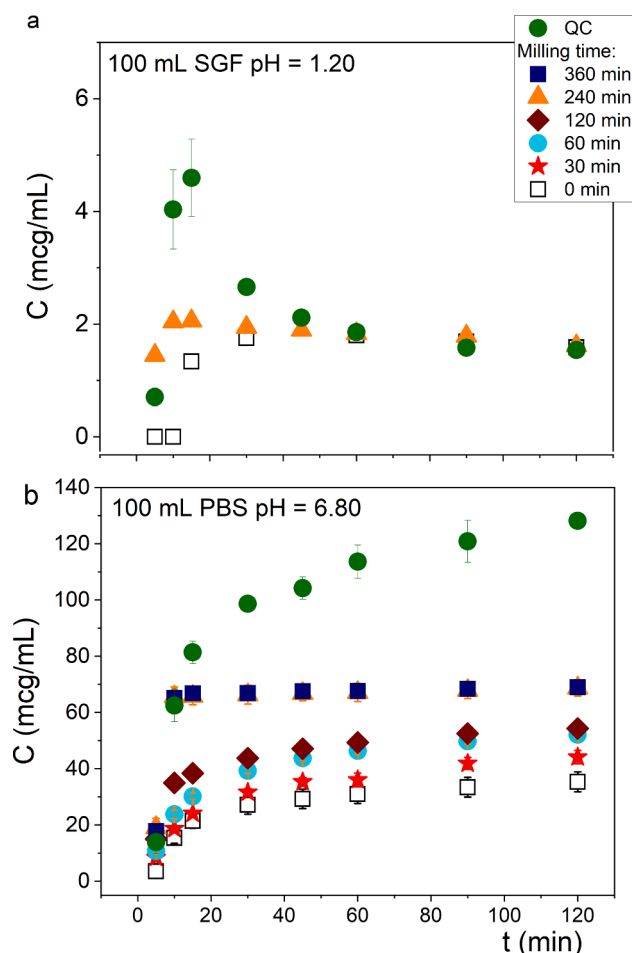
From a chemical point of view, bosentan is a bis-pyrimidine triple ether derivative containing a sulfonamide moiety that plays an important role in the interaction with the endothelin receptor. The presence of the sulfonamide group in the structure is also responsible for the weak acidic properties of bosentan. According to information given in a European public assessment report (EPAR) of the drug product *Tracleer*, bosentan has a  $\text{pK}_a$  of 5.46. As a rule of thumb, an acidic drug is unionized at pH values up to 2 units below its  $\text{pK}_a$ , and completely ionized at pH values greater than 2 units above its  $\text{pK}$  (Florence and Attwood, 2016). Thus, bosentan is unionized below pH of 3.46 and fully ionized at a pH above 7.46. As a result, the saturation solubility of bosentan at 37 °C depends on pH and is the lowest in the gastric milieu (e.g. SGF pH = 1.20), i.e.  $1.95 \pm 0.11 \mu\text{g/mL}$  (Krupa et al., 2017b) where the ionization of the drug is below 0.009 %. When the dissolution of bosentan is tested at the SGF, non-sink conditions with a very small sink index (SI), i.e. 0.01 (Sun et al., 2016) are obtained. Under these conditions, the fully amorphous form of bosentan forms metastable supersaturated solutions, reaching the maximum concentration after 15 min

( $2.06 \pm 0.29 \mu\text{g/mL}$  –  $4.60 \pm 0.68 \mu\text{g/mL}$ ). Then, drug precipitation is observed (Fig. 6a). This desupersaturation is accompanied by a gradual color change in the tested samples. Before the dissolution test, all dry amorphous formulations are yellow, but after 2 h of dissolution studies in SGF, most of these particles turn white and look the same as the crude crystalline bosentan monohydrate. These findings are in line with a spring-and-parachute pattern of dissolution proposed by Sun et al., 2016 for poorly soluble drugs studied in extremely nonsink conditions.

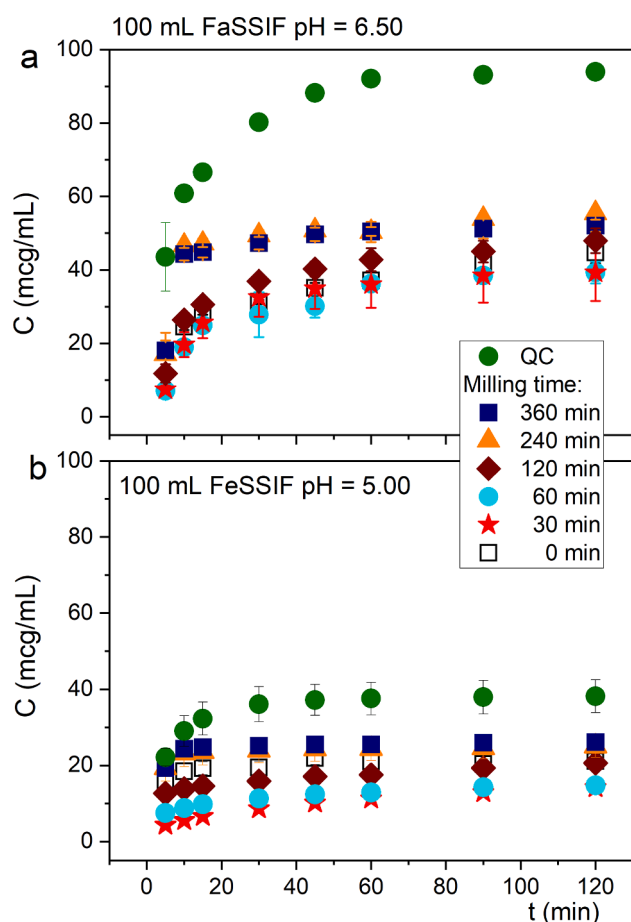
In contrast to SGF, the equilibrium solubility of bosentan in the intestinal environment sharply increases to reach the value of  $41.56 \pm 0.48 \mu\text{g/mL}$  in PBS of pH = 6.80,  $37.73 \pm 3.31 \mu\text{g/mL}$  in FaSSIF of pH = 6.50 and  $21.04 \pm 2.76 \mu\text{g/mL}$  in FeSSIF of pH = 5.00. These results are related to an increase in the ionization percentage with an increase in the pH of the solvent.

Fig. 6b shows the concentration–time profiles of ball milled bosentan determined using PBS, while the dissolution profiles recorded using biorelevant fluids, i.e. FaSSIF and FeSSIF are presented in Fig. 7. For comparison, the concentration–time profiles typical of the crude drug are presented as well.

When PBS is used for dissolution studies, the concentration of bosentan dissolved gradually increases with time (Fig. 6b), but after 120 min of this test, drug precipitation is not observed. It could be related to the high percentage of ionized bosentan at pH = 6.80, that is, 95% and more than twenty times higher SI, that is, 0.21. Moreover, the concentration of bosentan dissolved gradually increases with increasing milling



**Fig. 6.** Influence of amorphization method, i.e. quenched cooling (QC, green circles) or ball milling on concentration–time profiles of bosentan dissolved in non-sink conditions using: (a) SGF of pH = 1.2; (b) PBS of pH = 6.80. (For interpretation of the references to color in this figure legend, the reader is referred to the web version of this article.)



**Fig. 7.** Influence of amorphization method, i.e. quenched cooling (QC, green circles) or ball milling on concentration–time profiles of bosentan dissolved in non-sink conditions using biorelevant fluids: (a) FaSSiF of pH = 6.50; (b) FeSSiF of pH = 5.00. (For interpretation of the references to color in this figure legend, the reader is referred to the web version of this article.)

time. In the end of the study, the amount of bosentan dissolved reaches the maximum values of  $68.67 \pm 2.88 \mu\text{g/mL}$  or  $68.97 \pm 1.76 \mu\text{g/mL}$  for fully amorphous formulations, such as those ball milled for 4 or 6 h respectively. These values are twice higher than those recorded for the crude bosentan.

Unlike PBS, the biorelevant fluids contain mixed micelles-forming surfactants typical of the intestinal environment [FaSSiF: taurocholate 3 mM (bile salts), phospholipids 0.75 mM; FeSSiF: taurocholate 15 mM (bile salts), phospholipids 3.75 mM]. The surface tension determined at room temperature is  $51.7 \pm 2.5 \text{ mN/m}$  for FaSSiF and  $48.6 \pm 0.4 \text{ mN/m}$  for FeSSiF (data kindly provided by Biorelevant.com). Yet, similarly to the results obtained in the PBS, the percentage of ionization together with the milling time govern the shape of dissolution profiles more than the load of surface active compounds in these solvents. Thus, more than twice higher amount of bosentan dissolves in FaSSiF of a pH = 6.50 and ionization = 95 % (SI = 0.19) than in FeSSiF of a pH = 5.00 and ionization = 90 % (SI = 0.11). Fully amorphous samples show the most favorable dissolution profiles. After 120 min,  $55.48 \pm 0.67 \mu\text{g/mL}$  or  $52.07 \pm 1.63 \mu\text{g/mL}$  of bosentan dissolve in FaSSiF from samples milled for 4 or 6 h, respectively. When these samples are analyzed in FeSSiF, the concentration of bosentan dissolved is twice lower than in FaSSiF, and ranges from  $24.98 \pm 2.85 \mu\text{g/mL}$  to  $26.09 \pm 0.56 \mu\text{g/mL}$ .

Interestingly, the supersaturation reached when quenched cooled samples are examined is much higher than that typical of ball milled bosentan regardless of the solvent used for dissolution testing (Figs. 6–7). Thus, not only the milling time, but also the method used for the

amorphization/vitrification of the drug could determine the drug dissolution rate.

The impact of the amorphization method on the intrinsic dissolution of bosentan was described by Minecka et al., 2022. Although using 1.0 % sodium dodecyl sulfate as a dissolution solvent, the authors showed that quenched cooled bosentan dissolved more rapidly, reaching concentrations higher than those recorded for cryomilled formulations. Taking into account the results of thermal and dielectric studies, the authors suggested that the cryomilled bosentan might be more physically stable than quenched cooled samples, and therefore its dissolution rate was slower.

This phenomenon might also be related to the electrostatic forces responsible for the agglomeration of fine particles of amorphous bosentan prepared by high energy ball milling (Zimper et al., 2010), which was not observed when a brittle quenched cooled bosentan glass was gently ground in a mortar (Fig. 8 b, d).

### 3.5. Amorphous bosentan re-crystallized in water at 37 °C

To understand better, the properties of bosentan precipitating from supersaturated solutions, monohydrate bosentan samples milled for 0, 10, 30, 240 and 360 min were suspended in water (1:3 w/w). These suspensions were kept for 72 h at 37 °C. Then, the solid particles were filtered and dried at 40 °C for 24 h using a glass oven type B-585 (Büchi Labortechnik AG, Flavil, Switzerland). These solid particles (called SP0, SP10, SP30, SP240 and SP360) were then analyzed by SEM, XRD and DSC.

The morphology of recrystallized particles prepared using fully amorphous bosentan (SP240) was compared to the original ball milled sample and the crude drug in Fig. 8. After 240 min of high energy ball milling, the original size of crystalline particles of bosentan [ $d_{50} = 102 \mu\text{m}$  (Krupa et al., 2017b)] was reduced about ten times ( $n = 20$ , Fig. 8 a–b). In turn, the recrystallized sample was formed of agglomerated tiny particles which were much smaller than those visible in the image of the original ball milled sample (Fig. 8 b–c). Inside these agglomerates (Fig. 8 c), single microcrystals, rod- and plate-shaped, are visible.

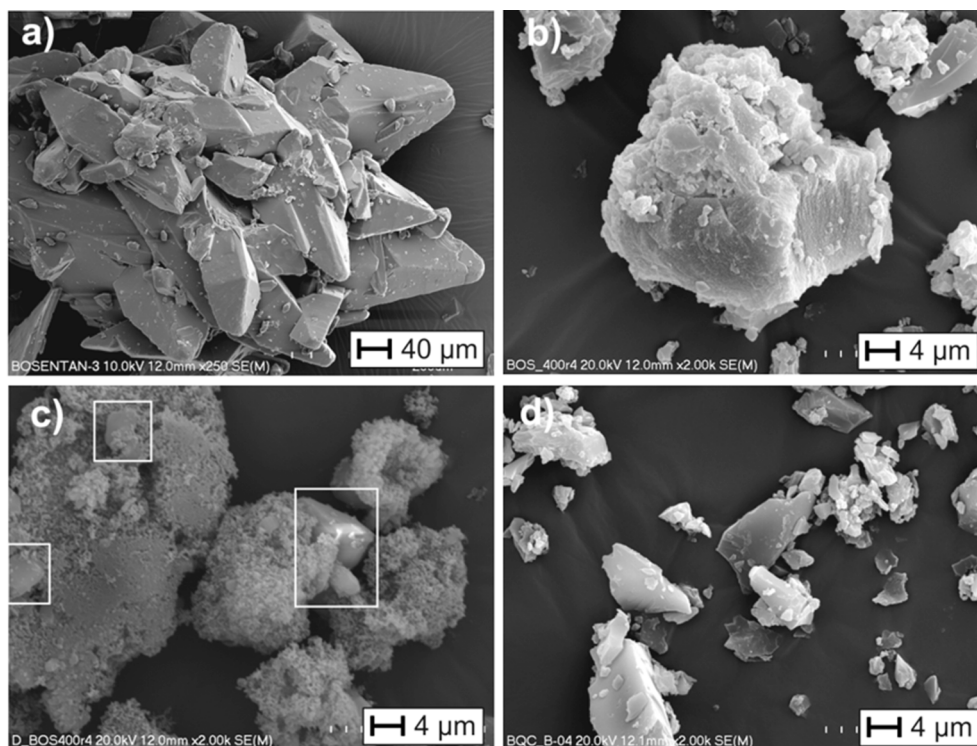
Fig. 9 shows the X-ray diffraction patterns of semi-amorphous (milling time = 30 min) and fully amorphous bosentan (milling time = 240 min) recorded just before, and just after its dissolution and recrystallization in water. The diffractograms of both the monohydrate and the anhydrous crystalline form of bosentan are also reported for comparison. In both cases, it appears that the recrystallization in water, which follows the dissolution of the milled samples (30 min or 240 min), leads to the monohydrate form.

Fig. 10 shows the heating (5 °C/min) DSC scans of solid particles obtained after dissolution in water of monohydrate bosentan samples milled for 0, 10, 30, 240 and 360 min. All thermograms show an endothermic peak ranging from 40 to 80 °C, signaling the dehydration of the monohydrate. At higher temperatures (90 °C, 120 °C), we observe two overlapping endotherms, corresponding to the melting of anhydrous bosentan, arising from the dehydration of milled and non-milled bosentan monohydrate (see Fig. 4). This bimodal melting, thus, reflects a bimodal crystallite size distribution with smaller crystallites melting at lower temperatures. We can note that the two endothermic components have antagonist evolutions. Interestingly, the first one increases for increasing milling times while the second one decreases. This indicates that the longer the milling the smaller the size of the particles, which recrystallize in water.

## 4. Conclusions

An anhydrous form of bosentan was obtained by dehydration of the monohydrate and described for the first time. This anhydrous form was found to be unstable at RT and went back rapidly toward the monohydrate form under ambient atmosphere. Moreover, no sign of amorphization could be detected upon dehydration whatever the





**Fig. 8.** SEM images recorded for: (a) crude bosentan monohydrate – crystalline form; (b) bosentan monohydrate ball milled for 240 min – amorphous form; (c) bosentan monohydrate ball milled for 240 min and recrystallized in water at 37 °C, inside rectangles big crystals were shown; (d) quenched cooled glass of bosentan ground in mortar.

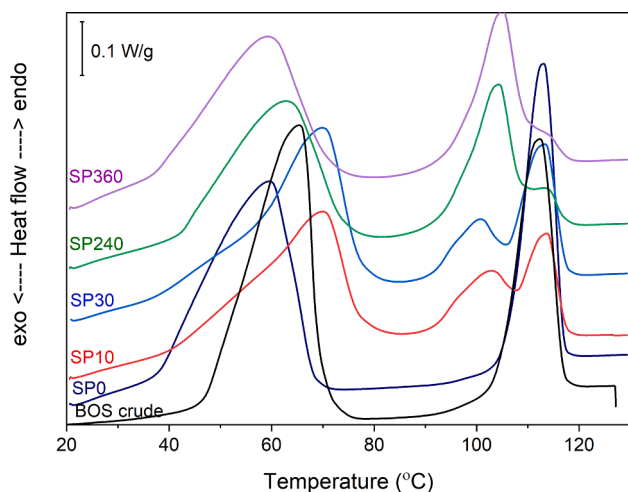


**Fig. 9.** XRD patterns of bosentan monohydrate (BOS) milled for either 30 min (BOS30) or 240 min (BOS240) and those of the particles recrystallized in water at 37 °C, i.e. SP30 and SP240 respectively. All diffractograms were recorded at RT.

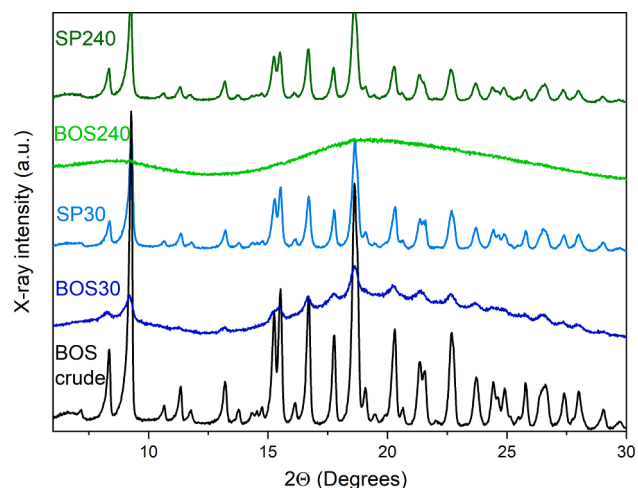


**Fig. 10.** Heat flow curves (5 °C/min) of ball milled semi-amorphous SP10, SP30 or amorphous SP240, SP360 bosentan monohydrate (BOS) recrystallized in water at 37 °C; unmilled drug dried after suspending in water (SP0) together with that of crude BOS are shown for comparison.

dehydration protocol was (fast or slow).

Two amorphous bosentan forms ( $T_g = 82$  °C) could be produced by melt quenching and high energy milling without any noticeable chemical degradation. Interestingly, neither of them recrystallizes while heating up to 190 – 250 °C revealing the high physical stability of this form. Moreover, in the case of milling, this high stability was also effective in the course of the amorphization process itself when the amorphization was only partial. This very exceptional property makes bosentan a model system to study the physics of solid state amorphization upon milling.

Dissolution studies carried out in either SGF, PBS or biorelevant

fluids (FaSSiF, FeSSiF) showed the beneficial effect of amorphization on the concentration of bosentan dissolved. When SGF was used, the precipitation of the amorphous drug started only after 30 min of the test. On the other hand, there was no precipitation observed in either PBS, FaSSiF or FeSSiF. The DSC and XRD results confirmed that when ball milled bosentan was suspended in water at 37 °C, it started to transform into the crystalline monohydrate. Importantly, the vitrification of bosentan was followed by a reversible color change from creamy-white to yellow. When the amorphous form recrystallized in the aqueous environment, the samples regained their creamy-white color.

Since the solubility of bosentan depended on pH, further studies



would be necessary to elucidate the impact that both temperature and pH of the solvent may have on the kinetics of nucleation and growth of crystals in the amorphous systems of bosentan in aqueous solutions.

#### CRediT authorship contribution statement

**Anna Krupa:** Conceptualization, Investigation, Visualization, Validation, Writing – original draft, Writing – review & editing, Funding acquisition, Project administration, Supervision. **Florence Danède:** Investigation, Methodology. **Agnieszka Węgrzyn:** Investigation, Methodology. **Dorota Majda:** Investigation, Methodology. **Jean-François Willart:** Conceptualization, Methodology, Validation, Writing – original draft, Writing – review & editing, Supervision.

#### Declaration of Competing Interest

The authors declare that they have no known competing financial interests or personal relationships that could have appeared to influence the work reported in this paper.

#### Acknowledgements

The research was performed thanks to Sonata Bis grant no DEC-2019/34/E/NZ7/00245 financed by the National Science Centre in Poland and BGF-Séjour scientifique ed. 2020 grant funded by the French Embassy in Poland on behalf of the French Government.

#### Appendix A. Supplementary material

Supplementary data to this article can be found online at <https://doi.org/10.1016/j.ijpharm.2022.121846>.

#### References

- Álvarez Reyes, F., Luna Gómez, C., Brito Suárez, M., 2011. Effect of the dual endothelin receptor antagonist bosentan on untreatable skin ulcers in a patient with diabetes: a case report. *J. Med. Case Rep.* 5, 151. <https://doi.org/10.1186/1752-1947-5-151>.
- Amann-Winkel, K., Gainaru, C., Handle, P.H., Seidl, M., Nelson, H., Böhrer, R., Loerting, T., 2013. Water's second glass transition. *Proc. Natl. Acad. Sci.* 110, 17720–17725. <https://doi.org/10.1073/pnas.1311718110>.
- Bhugra, C., Shmeis, R., Pikal, M.J., 2008. Role of Mechanical Stress in Crystallization and Relaxation Behavior of Amorphous Indomethacin. *J. Pharm. Sci.* 97, 4446–4458. <https://doi.org/10.1002/jps.21291>.
- Dudognon, E., Danède, F., Descamps, M., Correia, N.T., 2008. Evidence for a New Crystalline Phase of Racemic Ibuprofen. *Pharm. Res.* 25, 2853–2858. <https://doi.org/10.1007/s11095-008-9655-7>.
- Elisei, E., Willart, J.-F., Danède, F., Siepmann, J., Siepmann, F., Descamps, M., 2018. Crystalline Polymorphism Emerging From a Milling-Induced Amorphous Form: The Case of Chlorhexidine Dihydrochloride. *J. Pharm. Sci.* 107, 121–126. <https://doi.org/10.1016/j.xphs.2017.07.003>.
- Enevoldsen, F.C., Sahaana, J., Wehland, M., Grimm, D., Infanger, M., Krüger, M., 2020. Endothelin Receptor Antagonists: Status Quo and Future Perspectives for Targeted Therapy. *J. Clin. Med.* 9, 824. <https://doi.org/10.3390/jcm9030824>.
- Florence, A.T., Attwood, D., 2016. *Physicochemical Principles of Pharmacy In Manufacture, Formulation and Clinical Use*, Sixth. ed. Royal Pharmaceutical Society, London.
- Fong, S.Y.K., Bauer-Brandl, A., Brandl, M., 2017. Oral bioavailability enhancement through supersaturation: an update and meta-analysis. *Expert Opin. Drug Deliv.* 14, 403–426. <https://doi.org/10.1080/17425247.2016.1218465>.
- Galwey, A.K., 2000. Structure and order in thermal dehydrations of crystalline solids. *Thermochim. Acta* 355, 181–238. [https://doi.org/10.1016/S0040-6031\(00\)00448-2](https://doi.org/10.1016/S0040-6031(00)00448-2).
- Garnier, S., Petit, S., Coquerel, G., 2002. Dehydration mechanism and crystallisation behaviour of lactose. *J. Therm. Anal. Calorim.* 68, 489–502. <https://doi.org/10.1023/A:1016087702409>.
- Garnier, S., Petit, S., Mallet, F., Petit, M.-N., Lemarchand, D., Coste, S., Lefebvre, J., Coquerel, G., 2008. Influence of ageing, grinding and preheating on the thermal behaviour of  $\alpha$ -lactose monohydrate. *Int. J. Pharm.* 361, 131–140. <https://doi.org/10.1016/j.ijpharm.2008.05.023>.
- Gordon, J.M., Rouse, G.B., Gibbs, J.H., Risen, W.M., 1977. The composition dependence of glass transition properties. *J. Chem. Phys.* 66 (11), 4971–4976.
- Gutzow, I. S., Mazurin, O. V., Schmelzer, J. W. P., Todorova, S. V., Petroff, B. B., Privén, A.I., 2011. *Glasses and the Glass Transition*. Wiley.
- Hostenbach, S., Pauwels, A., Michiels, V., Raeymaekers, H., Van Binst, A.-M., Van Merhaeghen-Wieleman, A., Van Schuerbeek, P., De Keyser, J., D'Haeseleer, M., 2019. Role of cerebral hypoperfusion in multiple sclerosis (ROCHIMS): study protocol for a proof-of-concept randomized controlled trial with bosentan. *Trials* 20, 164. <https://doi.org/10.1186/s13063-019-3252-4>.
- Javor, S., Salsano, A., 2020. Why not consider an endothelin receptor antagonist against SARS-CoV-2? *Med. Hypotheses* 141, 109792. <https://doi.org/10.1016/j.mehy.2020.109792>.
- Kaur, M., Jasinski, J.P., Keeley, A.C., Yathirajan, H.S., Betz, R., Gerber, T., Butcher, R.J., 2013. Bosentan monohydrate. *Acta Crystallogr. Sect. E Struct. Reports Online* 69, o12–o13. <https://doi.org/10.1107/S1600536812048969>.
- Kefford, R., Clingan, P.R., Brady, B., Ballmer, A., Morganti, A., Hersey, P., 2010. A randomized, double-blind, placebo-controlled study of high-dose bosentan in patients with stage IV metastatic melanoma receiving first-line dacarbazine chemotherapy. *Mol. Cancer* 9 (1), 69.
- Kendre, P.N., Chaudhari, P.D., Jain, S.P., Vibhute, S.K., 2021. An effort to augment solubility and efficiency of the oral bosentan-bucco-adhesive drug delivery system using graft co-polymer as the carrier. *Polym. Bull.* 78, 5851–5871. <https://doi.org/10.1007/s00289-020-03412-z>.
- King, T.E., Brown, K.K., Raghu, G., du Bois, R.M., Lynch, D.A., Martinez, F., Valeyre, D., Leconte, I., Morganti, A., Roux, S., Behr, J., 2011. BUILD-3: A Randomized, Controlled Trial of Bosentan in Idiopathic Pulmonary Fibrosis. *Am. J. Respir. Crit. Care Med.* 184 (1), 92–99.
- Krupa, A., Cantin, O., Strach, B., Wyska, E., Tabor, Z., Siepmann, J., Wróbel, A., Jachowicz, R., 2017a. In vitro and in vivo behavior of ground tadalafil hot-melt extrudates: How the carrier material can effectively assure rapid or controlled drug release. *Int. J. Pharm.* 528, 498–510. <https://doi.org/10.1016/j.ijpharm.2017.05.057>.
- Krupa, A., Descamps, M., Willart, J.-F., Strach, B., Wyska, E., Jachowicz, R., Danède, F., 2016. High-Energy Ball Milling as Green Process To Vitrify Tadalafil and Improve Bioavailability. *Mol. Pharm.* 13, 3891–3902. <https://doi.org/10.1021/acs.molpharmaceut.6b00688>.
- Krupa, A., Majda, D., Mozgawa, W., Szlęk, J., Jachowicz, R., 2017b. Physicochemical Properties of Bosentan and Selected PDE-5 Inhibitors in the Design of Drugs for Rare Diseases. *AAPS PharmSciTech* 18, 1318–1331. <https://doi.org/10.1208/s12249-016-0599-7>.
- Minecka, A., Chmiel, K., Jurkiewicz, K., Hachula, B., Lunio, R., Żakowiecki, D., Hyla, K., Milanowski, B., Koperwas, K., Kamiński, K., Paluch, M., Kamińska, E., 2022. Studies on the Vitrified and Cryomilled Bosentan. *Mol. Pharm.* 19, 80–90. <https://doi.org/10.1021/acs.molpharmaceut.1c00613>.
- Ngono, F., Willart, J.-F., Cuello, G., Jimenez-Ruiz, M., Affouard, F., 2019. Lactulose: A Model System to Investigate Solid State Amorphization Induced by Milling. *J. Pharm. Sci.* 108, 880–887. <https://doi.org/10.1016/j.xphs.2018.09.013>.
- Panda, T., Das, D., Panigrahi, L., 2016. Formulation Development of Solid Dispersions of Bosentan using Gelucire 50/13 and Poloxamer 188. *J. Appl. Pharm. Sci.* 6, 027–033. <https://doi.org/10.7324/JAPS.2016.60904>.
- Petit, S., Coquerel, G., 1996. Mechanism of Several Solid–Solid Transformations between Dihydrated and Anhydrous Copper(II) 8-Hydroxyquinolates. Proposition for a Unified Model for the Dehydration of Molecular Crystals. *Chem. Mater.* 8, 2247–2258. <https://doi.org/10.1021/cm9600438>.
- Saleki-Gerhardt, A., Stowell, J.G., Byrn, S.R., Zograf, G., 1995. Hydration and Dehydration of Crystalline and Amorphous Forms of Raffinose. *J. Pharm. Sci.* 84, 318–323. <https://doi.org/10.1002/jps.2600840311>.
- Sanghavi, D.K., Titus, A., Caulfield, T.R., David Freeman, W., 2021. Endotheliitis, endothelin, and endothelin receptor blockers in COVID-19. *Med. Hypotheses* 150, 110564. <https://doi.org/10.1016/j.mehy.2021.110564>.
- Schittny, A., Huwyler, J., Puchkov, M., 2020. Mechanisms of increased bioavailability through amorphous solid dispersions: a review. *Drug Deliv.* 27, 110–127. <https://doi.org/10.1080/10717544.2019.1704940>.
- Sun, D.D., Wen, H., Taylor, L.S., 2016. Non-Sink Dissolution Conditions for Predicting Product Quality and In Vivo Performance of Supersaturating Drug Delivery Systems. *J. Pharm. Sci.* 105, 2477–2488. <https://doi.org/10.1016/j.xphs.2016.03.024>.
- Willart, J.F., Caron, V., Descamps, M., 2007. Transformations of crystalline sugars upon milling. *J. Therm. Anal. Calorim.* 90, 125–130. <https://doi.org/10.1007/s10973-007-8485-x>.
- Willart, J.F., Danède, F., De Gusseme, A., Descamps, M., Neves, C., 2003. Origin of the Dual Structural Transformation of Trehalose Dihydrate upon Dehydration. *J. Phys. Chem. B* 107, 11158–11162. <https://doi.org/10.1021/jp034679f>.
- Willart, J.F., De Gusseme, A., Hemon, S., Descamps, M., Leveiller, F., Rameau, A., 2002. Vitrification and polymorphism of trehalose induced by dehydration of trehalose dihydrate. *J. Phys. Chem. B* 106, 3365–3370. <https://doi.org/10.1021/jp012836+>.
- Willart, J.F., Dudognon, E., Mahieu, A., Eddleston, M., Jones, W., Descamps, M., 2017. The role of cracks in the crystal nucleation process of amorphous griseofulvin. *Eur. Phys. J. Spec. Top.* 226, 837–847. <https://doi.org/10.1140/epjst/e2016-60358-y>.
- Zimper, U., Aaltonen, J., Krauel-Goellner, K., Gordon, K.C., Strachan, C.J., Rades, T., 2010. The Influence of Milling on the Dissolution Performance of Simvastatin. *Pharmaceutics* 2, 419–431. <https://doi.org/10.3390/pharmaceutics2040419>.